A novel connection for fibre reinforced polymer bridge decks: Conceptual design and experimental investigation

A NOVEL CONNECTION FOR FIBRE REINFORCED POLYMER BRIDGE DECKS: CONCEPTUAL DESIGN AND EXPERIMENTAL INVESTIGATION

V. Mara[1], M. Al-Emrani[2], and R. Haghani[3]

ABSTRACT

In the past two decades, the use of fibre reinforced polymer (FRP) decks has attracted a great deal of attention when it comes to the refurbishment of existing bridges and the construction of new ones. FRP materials offer superior properties, such as high specific strength and stiffness, light weight, high fatigue and corrosion resistance and good durability. Because of their low self-weight and prefabrication potential, FRP composites lend themselves to accelerated bridge construction, thereby leading to minimised traffic interference. However, one challenge that is posed by FRP deck systems is the detailing and design of panel level connections. Today, a common practice for joining deck panels on site is adhesive bonding, which compromises the benefit of rapid FRP deck installation due to the time-restricted curing required for structural adhesives. As a result, there is a need for the development of joints which enable more rapid assembly. In this paper, a novel joint configuration for panel level connections is proposed. Numerical analyses and static experimental tests were conducted to evaluate the behaviour and load-carrying capacity of the connection. The overall investigation showed that the presented joint concept is a potential alternative for panel level connections in FRP decks.

Keywords: Bridge; Connection; Deck; Experiment; FRP; Panel level connection

1. Introduction

Fibre reinforced polymer (FRP) bridge decks have been recognised as a competitive alternative to traditional decking solutions for the refurbishment of existing bridges, as well as the construction of new ones [1-14]. FRP decks are characterised as light, strong, corrosion-resistant decks. The high degree of prefabrication enables the production of modular deck segments which can be easily transported and rapidly installed on site. Today, rapid on-site assembly has become a necessity, particularly in large cities, where the construction and maintenance of bridges often have a significant social, environmental and financial impact, including traffic disruption, noise pollution, carbon footprint and increased user costs, to mention just a few [15].

Rapid on-site assembly is highly dependent on the detailing and design of connections between the prefabricated bridge elements. These connections need to be detailed to facilitate a rapid, secure installation process, which calls, among other things, for generous tolerances. At the same time, it should be noted that a good fit between different prefabricated elements is required to ensure safe, durable joints. Today, a common practice for joining FRP deck panels on site to form the entire deck involves

[1] PhD student, Dept. of Civil and Environmental Engineering, Division of Structural Engineering, Chalmers University of Technology, Sven Hultins gata 8, SE-412 96 Göteborg, Sweden
Tel. +46 31 772 20 19, E-mail: valbona.mara@chalmers.se
[2] Associate Professor, Dept. of Civil and Environmental Engineering, Division of Structural Engineering, Chalmers University of Technology, Sven Hultins gata 8, SE-412 96 Göteborg, Sweden
[3] Assistant Professor, Dept. of Civil and Environmental Engineering, Division of Structural Engineering, Chalmers University of Technology, Sven Hultins gata 8, SE-412 96 Göteborg, Sweden

the use of adhesively bonded connections. Mechanical connections, such as shear key connections, have also been used for this purpose, but these connections have shown sensitivity to traffic load and load transfer. Cracking in the shear key connection region after a short period of exposure to highway vehicle loads, as well as difficulty transferring the load from one deck panel to the other, has been the result of several constructed projects [16-18].

Adhesively bonded connections have proven to be efficient in load transfer, as well as fatigue resistance, but several challenges are encountered in conjunction with these connections on site:

- The time needed for the adhesive bond to cure and develop full strength (usually 48 h) compromises the benefit of rapid FRP deck installation.
- The quality control of adhesive joints in the field is fairly difficult.
- Dismantling these connections is impossible. In the event of partial deck damage due to accidents, impact loading, vandalism and so on, it is fairly difficult to replace the deck partially. The replacement of the entire deck might therefore be needed, leading to very costly repair strategies.
- On-site bonding requires that special consideration is taken when it comes to the health of workers when they handle adhesives due to injuries that might be caused through skin contact.
- On-site bonding should be performed in a controlled environment taking account of temperature, humidity and so on. If the weather is not conducive, the erection of tents with a controlled environment might cause a delay in the construction of bridges.

The aforementioned shortcomings of on-site adhesive bonding illustrate the need to develop alternative panel level connections for FRP decks. In this paper, a novel joint for panel level connections which enables rapid, straightforward, on-site assembly is proposed. A conceptual design for the connection is first introduced. The connection concept was designed and examined using the finite element (FE) method. Finally, static experimental tests were conducted to verify the response of the connection in the serviceability limit state and evaluate the load-carrying capacity and the failure mode of the proposed connection. The load and displacement relationship, flexural resistance and strain distributions were measured during the test.

2. Conceptual design

The detailing of connections in FRP decks is a somewhat complex process, which should take account of not only the structural performance and durability of the joint, but also the ease of application and the tolerances this necessitates. It should therefore be regarded as a process in which the bridge client, the designer, the manufacturer and the contractor are all involved. This process was applied in the design of the connection concept presented in this study. Among various criteria considered in the development of the connection concept, the most important ones were identified as: (i) allow for rapid bridge construction with no-skill labour and (ii) provide quick repair and replacement of the bridge deck panels. In addition, constraints such as material, cost and geometric shape were defined and taken into account in the development of the connection concept.

The geometry and shape of the developed connection concept is shown in Fig. 1. The concept is based on the mechanical interlocking of the two modules of the connection

sliding into one another at an angle of 45°. A tongue-and-groove mechanism is used in the connection to ensure full mechanical contact between the two modules. The difference in length of the tongues and grooves was opted for the ease of manufacturing and on-site assembly.

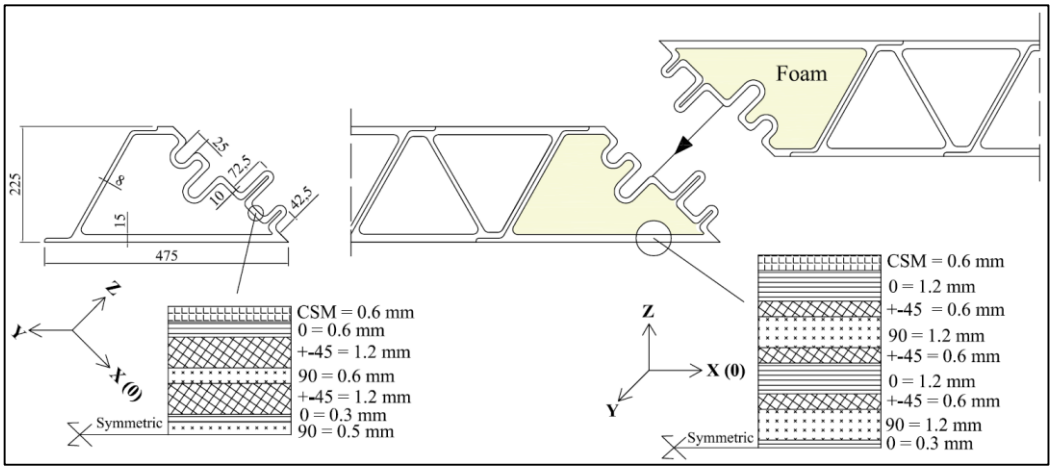

Fig.1. Geometry and dimensions of the connection module and the fibre architecture; CSM: continuous strand mat.

The cells of the connection modules were filled with PVC foam, Divinycell type H80, a product of DIAB. The mechanical properties of the foam are given in Table 1. The main function of the foam was to serve as a mould for the production of the connection modules in the vacuum infusion process (refer to Section 4.1). In addition to this, the foam provides support to the flanges and the grooves, which is translated to an increase in the patch load capacity and the bending capacity of the grooves. The ability of the foam to increase the capacity of foam filled cells has also been observed by Zi et al. [19].

Table 1. Mechanical properties of the foam.

Density	Compressive strength	Compressive modulus	Tensile strength	Tensile modulus	Shear strength	Shear modulus
(kg/m^3)	(MPa)	(MPa)	(MPa)	(MPa)	(MPa)	(MPa)
80	1.4	90	2.5	95	1.15	27

The ASSET FRP deck [20] – a product from Fiberline Composites, Denmark – was utilised in this study; the shape of the connection module was therefore designed to adapt to the ASSET deck profile. According to this concept, the connection modules are bonded to the FRP deck panels off site and assembled on site.

The fibre architecture of the connection was designed using the finite element (FE) method adopting the principal stress optimisation theory. The idea behind principal stress optimisation is to match the fibre directions and proportions with the principal stress vectors and stress magnitudes. In addition to this, other criteria were followed such as:

- E-glass and epoxy were selected for the fibres and the resin respectively. The reason for selecting E-glass fibres was their compatibility with the ASSET deck material, as well as cost constraints.

- For ease of manufacturing, the fibre directions were limited to 0^o, $\pm 45^o$ and 90^o.
- Symmetric laminates were used to avoid warpage and twisting from residual stresses
- To obtain a robust structure, 10% more fibres were provided in each direction. In addition, plies in 0^o, $\pm 45^o$ and 90^o angle were included in all the parts of the connection to account for unexpected loads.

A final design of the ply stack-up sequence is presented in Fig. 1.

3. Finite element modelling

3.1 FE model

Once the dimensions and the fibre architecture of the connection module had been determined, a global model utilising the commercially available ABAQUS 6-11.3 software was used to analyse the global behaviour and the load transfer mechanism of the connection, cf. Fig. 2. The model consisted of two FRP deck panels (ASSET deck) and the connection modules, all modelled with shell elements. The connection modules were filled with foam material that was modelled using solid elements with isotropic material properties with an elasticity modulus of E = 90 MPa and a Poisson ratio of 0.2. The shell elements of the connection were connected to the solid elements of the foam using surface-based, shell-to-solid coupling constraints.

As a result of the symmetry, half the model was modelled to minimise the number of finite elements. The boundary conditions were applied as simply supported, indicated in Fig. 2. The interaction between the surfaces of the connection modules was modelled with surface-to-surface contact elements with properties of frictionless tangential behaviour and hard contact normal behaviour, where separation after contact was allowed. In reality, friction between the connection modules is present. In this study, due to the absence of the coefficient of friction between the connection modules, frictionless contact was assumed. Based on this assumption, the FE results remain on the safe side, since the friction can enhance the performance of the connection. A finer mesh was used for the connection modules, as noted in Fig. 2. The mesh sizes gradually change from 10 mm in the middle to 50 mm towards the edges. In addition, it was made sure that the mesh density of the slave surface in the contact pair was finer than that of the master surface.

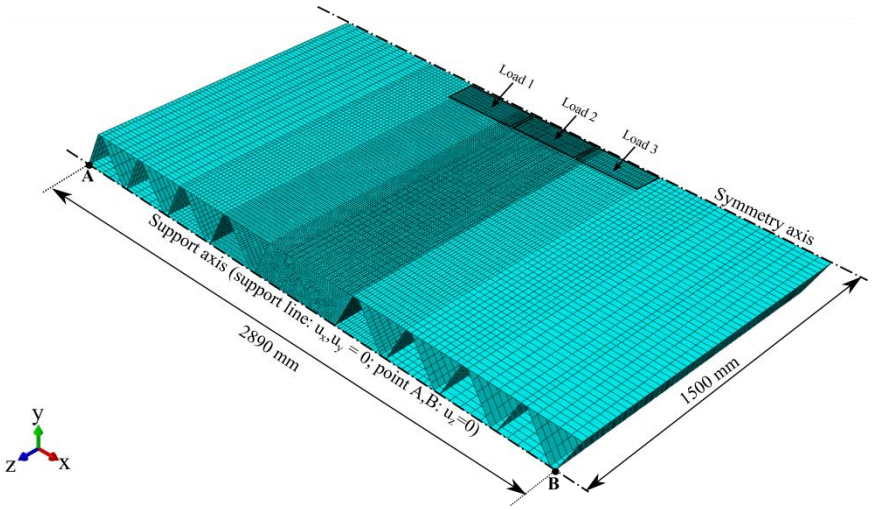

Fig. 2. Configuration of the FE model, the loading positions and the boundary conditions.

The ASSET deck profiles were modelled as lamina with the orthotropic material parameters defined in Table 2. The connection module was modelled as a composite lay-up with the designed fibre architecture. The material properties of a unidirectional (UD) E-glass-epoxy lamina in the connection module were determined by mathematical models considering a fibre volume fraction of 52% and are tabulated in Table 2. Based on the designed ply stack-up, the equivalent bending elastic properties for the flanges and grooves were also computed using the classical lamination theory (CLT) [21] and are summarised in Table 2 (refer to Fig. 1 for the reference coordinate system of the connection module). The model was loaded at three different loading positions, which were deemed as the most critical for the connection (see Fig. 2). The selected load configuration represents one wheel load according to EN 1991-2 [22], which is applied to an area of 400 x 400 mm^2.

Table 2. The mechanical properties used for the finite element modelling.

Property	ASSET deck			Connection module		
	Flange plates	Outer web plates	Inner web plates	Ply (UD glass-epoxy lamina)	Flanges	Tongues and grooves
E_x [MPa]*	23000	17300	16500	37000	23300	19300
E_y [MPa]	18000	22700	25600	10000	17200	15100
G_{xy} [MPa]	2600	3150	2000	4500	6900	8500
G_{xz} [MPa]	600	600	600	4500	-	-
G_{yz} [MPa]	600	600	600	2900	-	-
ν_{xy}	0.3	0.3	0.3	0.26	0.28	0.39

*X: pultrusion or fibre direction, Y: transverse direction for the ASSET deck and the glass-epoxy lamina in the connection module

3.2 Results from the FE model

Three load cases in accordance with the load positions shown in Fig. 2 were analysed. For each load case, a load of 150 kN equivalent to a wheel load in the serviceability limit state (SLS) was applied and the deflections and stresses were checked in different parts of the model. The maximum deflections for each load case are summarised in Table 3; they were obtained under the loading area. The top flanges under the load patch experienced greater deflections due to the local bending of the thin flanges.

Eurocode does not specify the limits for the global deflection of bridge decks. In the analysis performed here, a limit of L/300 is deemed reasonable. The same limit has been suggested in several previous studies [23, 24]. In this study, the deflection limit of L/300 is 10 mm, as the span of the FE model is three metres (see Fig. 2). Compared with this deflection limit, the global deflections in the model (max. deflection – bottom flange in Table 3) were lower for the SLS load level.

Table 3. Results of the finite element models for each load case.

Load position	Max. deflection – bottom flange	Max. deflection – top flange	Openings – bottom flange of the connection modules
Load 1 – 150 kN	9.5 mm	14 mm	2 mm
Load 2 – 150 kN	9.8 mm	14 mm	2.1 mm
Load 3 – 150 kN	7.6 mm	12.8 mm	0.6 mm

Checking the stresses in the longitudinal and transverse directions in the ASSET deck and the connection module revealed that all the stresses were below the strength limits with a factor of at least 2. A direct conclusion from this observation was that the system would withstand the ULS load levels, as they are only 35% above the SLS limit in the Eurocode.

Apart from the global deflections and the stresses, the behaviour of the connection with respect to openings in the bottom flange due to loading was studied in the serviceability limit state (results presented in Table 3). Fig. 3 presents a schematic of the opening between the connection modules in load case 2. It was noted that the top flanges remain in contact, while the connection opened by 2.1 mm in the bottom part. The opening area was limited to the first tongue-groove connection in the bottom part (in Fig. 3), as the mechanical interaction of the tongue and the groove prevented further opening between the connection modules. This behaviour was observed for all load cases. In overall terms, the connection displayed satisfactory behaviour, as the top flanges did not open; this might otherwise represent a threat for wear surface cracking. In the following sections, other results from the FE analyses are discussed and compared with the measured results of the experimental test.

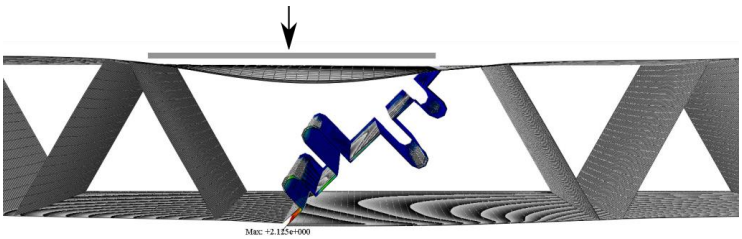

Fig. 3. Opening of the connection modules under load position 2.

4. Experimental investigation

4.1 Specimen and materials

To verify the performance of the proposed connection, experimental work including manufacturing and testing a large-scale specimen under static bending was carried out. The dimensions of the tested specimen are illustrated in Fig. 4. The length of the specimen was 3000 mm. The ASSET deck panels were manufactured using the pultrusion method, bonded by the manufacturer (Fiberline Composites, Denmark) and delivered to the laboratory.

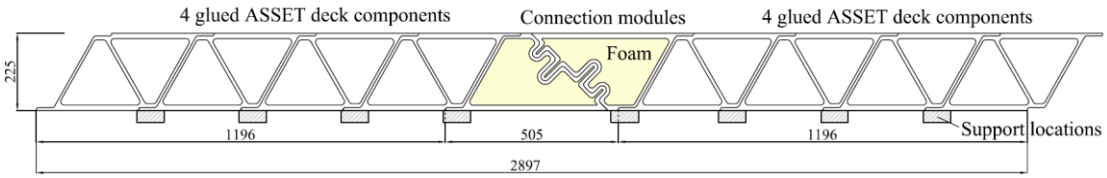

Fig. 4. Cross-section of the specimen.

The connection module was manufactured using the infusion method by Mostostal, Poland, and is shown in Fig. 5. Several challenges were encountered during the manufacture of the connection module:

- The designed ply stack-up sequence could not be followed by the manufacturer; instead, mats with chopped discontinuous fibres were used.
- The shape of the connection module was challenging for the infusion process and this led to mismatch and variable gaps between the two connection modules.
- The surfaces of the flanges were not plane but curved in different areas, resulting in some unsupported areas (gaps between the support and the specimen) during the tests.
- The thickness of the flanges varied from 8 to 10 mm.

Fig. 5. The connection modules made in the process of infusion.

The characterisation of the material properties for the connection module was only performed for the elastic modulus by testing plates using the longitudinal stress-wave frequency method. The elastic modulus of the composite material in the connection modules was the same in both the longitudinal and transverse directions, due to the used mats with chopped discontinuous fibres for production, and was estimated at 22.7 GPa. This elasticity modulus was within the range of the computed equivalent elastic properties of the laminates based on the designed ply stack-up sequence (refer to Table 2). Therefore, the effect of the material change in the FE analyses was trivial, which implied that the performed FE analyses were still valid and comparable with the tested specimen. The connection modules were then bonded to the ASSET deck panels in the laboratory using the SikaDur 330 epoxy adhesive type.

4.2 Experimental set-up and loading

The test set-up is shown in Fig. 6. The specimen was simply supported on two steel beams (VKR 150 x 150 x 5 profiles (S355)), one on each side of the specimen. A 10 mm thick steel plate was welded to the top flange of each steel beam to stiffen the flange. Between the steel beams and the specimen, eight rollers were positioned under the junction of the inclined webs of the specimen, at which the load transfer from the

specimen to the supports took place. Strain gauges were installed on the side of the rollers, as shown in Fig. 6, in order to measure the distribution of the reaction forces along the support lines. The rollers had an outer diameter of 70 mm, thickness of 5 mm and a length of 80 mm. The steel material used for the rollers was S355. In order to easily position and fit the rollers, steel plates were used on top of the rollers, as shown in Fig. 6. The maximum measurable reaction force on the rollers was approximately 30 kN before yielding took place in the steel material of the rollers. The rollers were calibrated before the loading of the specimen and the linear load-strain distribution was incorporated into the reaction force calculations. Due to the load limitation of the rollers, they were only used for the tests in SLS loading (see Table 4), while, for the final test, an elastic strip was placed between the specimen and the steel beams.

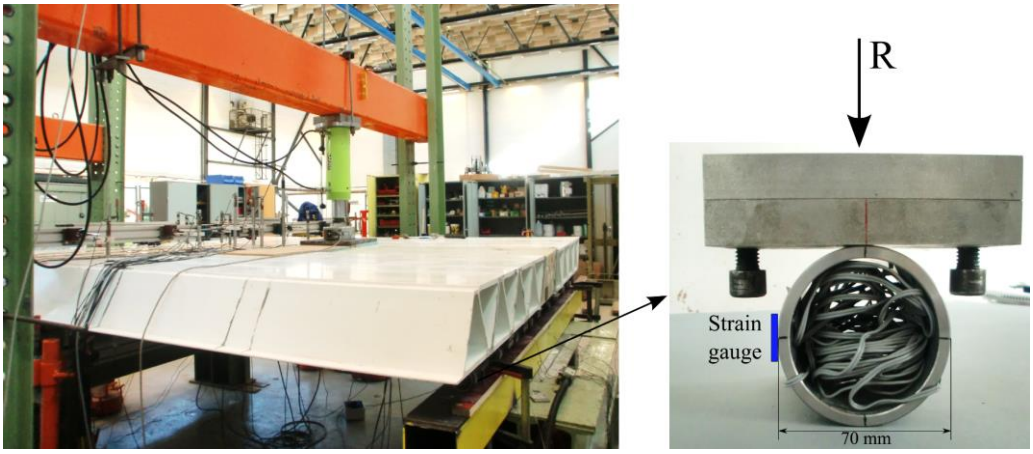

Fig. 6. Experimental set-up and support conditions.

The specimens were tested with concentrated loads in three different load positions, as indicated in Fig. 7. The load was applied with an hydraulic jack with a capacity of 450 kN. A steel plate with dimensions of 400 x 400 mm and a thickness of 25 mm was used for load distribution. A 15 mm thick timber plate with the same dimensions was placed between the steel plate and the specimen. Several studies [25-27] have demonstrated that the steel patch loading does not adequately represent the local effect of the tyre loads, which is much more important in fatigue loading. Instead, simulated tyre patch loads or curved metal plates have been suggested. However, in the absence of the suggested loading facilities, a steel patch load was used in this study. Thus, the local effects of the tyre loads were not appropriately captured in the tests.

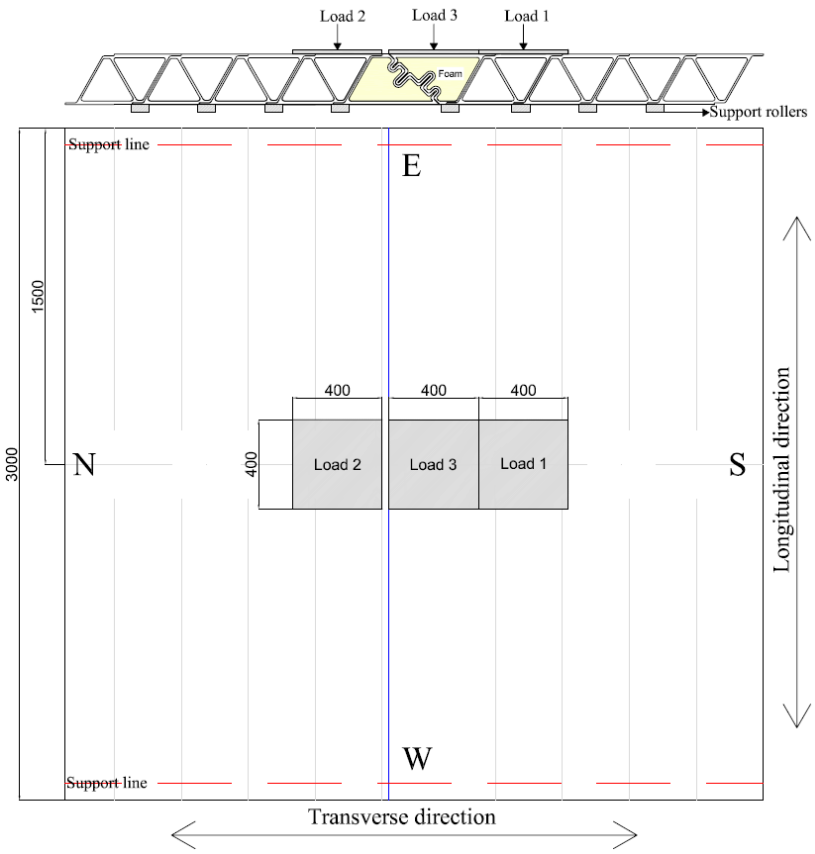

Fig. 7. Loading configuration of the test specimen.

The specimen was loaded consecutively (load 1, load 2 and load 3) up to the serviceability limit load of 150 kN. Afterwards, the specimen was loaded up to a maximum load of 433 kN in load position 3. An overview of all the experiments carried out within this study is presented in Table 4. The designation of the tests is used in the entire context of this paper. The tests were run with a displacement-controlled load at a rate of 0.25 mm/min. In every experiment, the applied loads, the vertical and horizontal deflections and the strain were measured in various locations described in Section 4.3.

Table 4. An overview of the performed tests.

Designation	**Test type**	**Maximum load (kN)**
T1-SLS	SLS load position 1	150
T2-SLS	SLS load position 2	150
T3-SLS	SLS load position 3	150
T3-Fail	Failure load position 3	> 433

4.3 Instrumentation

The deflections of the specimen were measured at several locations using linear variable displacement transducers (LVDT). The LVDTs were located on the top and bottom flanges of the specimen, with the pattern presented in Fig. 8 and Fig. 9, to measure the vertical and horizontal displacements (the latter to measure the openings

between the connection modules). Taking advantage of the symmetry, measurements were mainly concentrated in one half of the specimen. It should be noted that the LVDTs in the bottom plate were only used during SLS loading. A set of strain gauges was also installed on the top and bottom flanges of the specimen, as shown in Fig. 8 and Fig. 9.

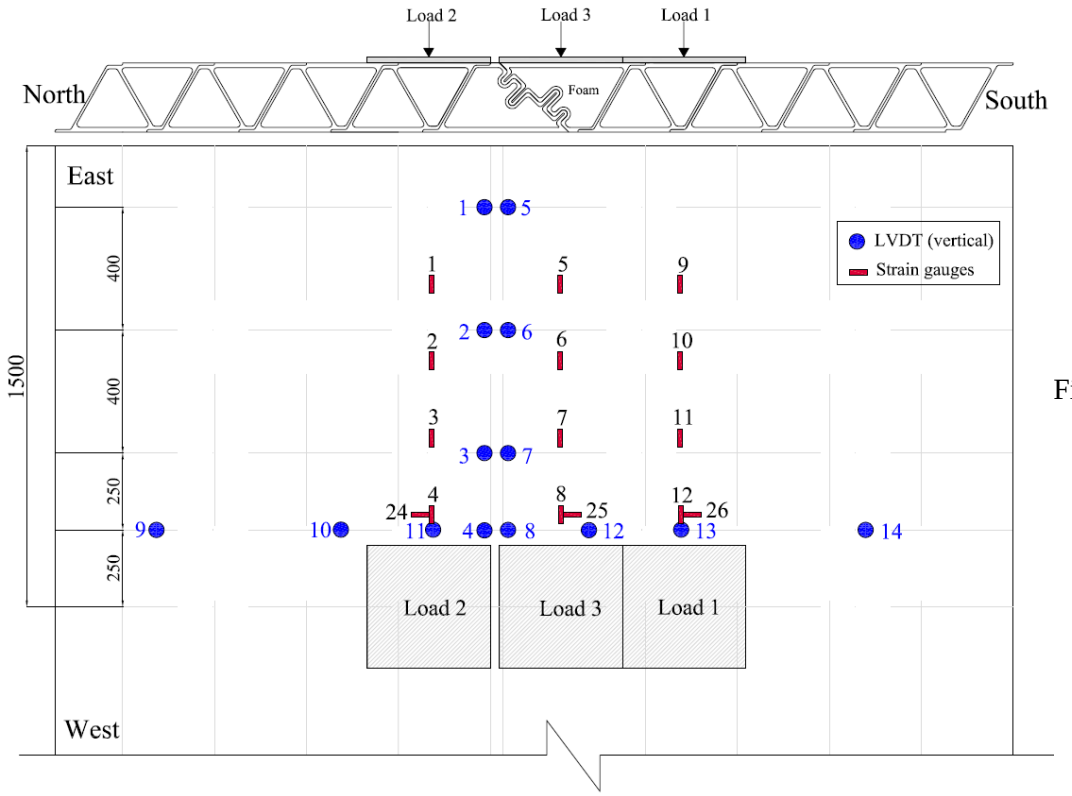

Fig 8. Displacement transducers (LVDTs) and strain gauges at the top flange.

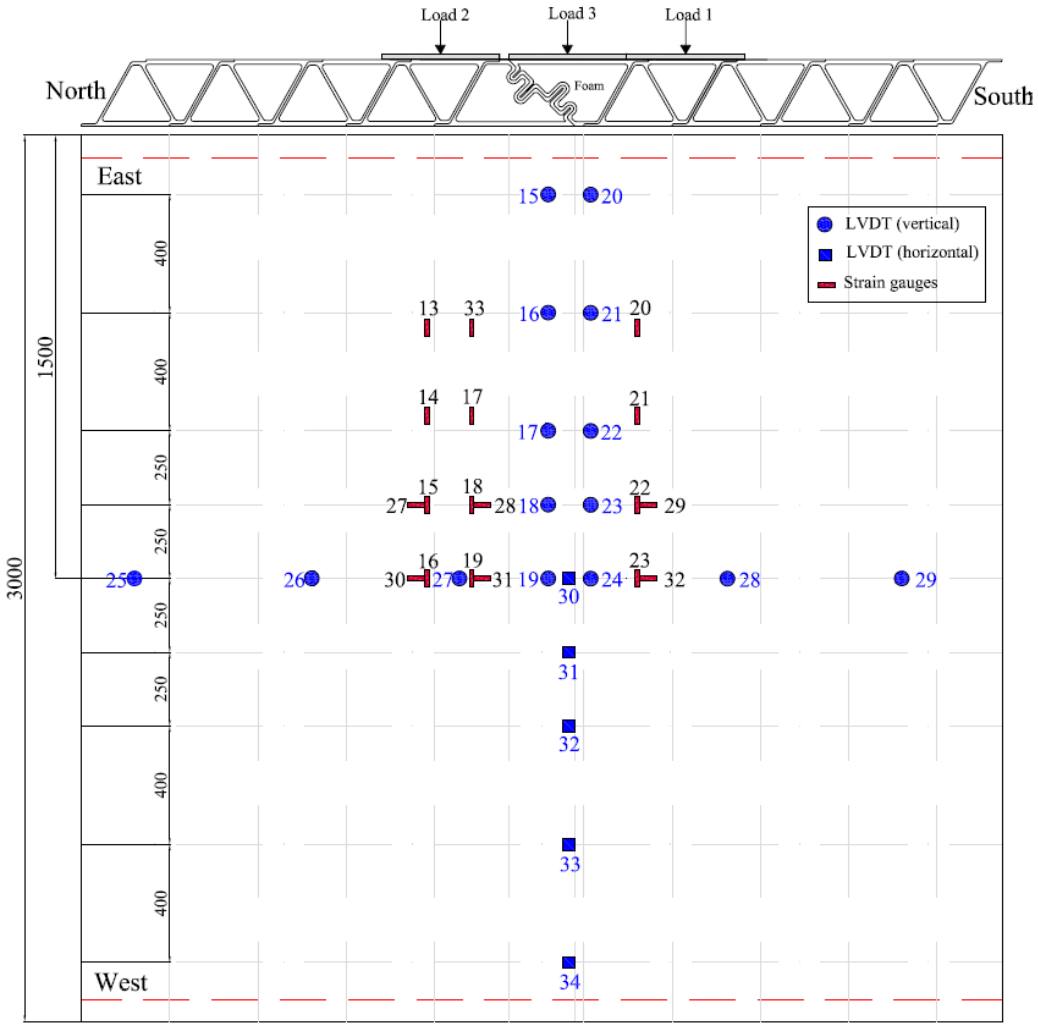

Fig. 9. Displacement transducers (LVDTs) and strain gauges at the bottom flange.

4.4 Results and discussion

4.4.1 Results of SLS tests

The maximum deflections on the top and bottom flanges of the specimen at a load of 150 kN, transverse to the span, are shown in Fig. 10 and Fig. 11 for all load cases. Some of the LVDTs did not provide results in a number of load cases. The deflection curves show a typical localised effect under the patch load and the north or south part of the specimen tended to lift up and display positive deflections depending on the load position. Comparing the three tests, it can be seen that load position 2 is critical for the connection, because large deformation incompatibilities are observed in the connection region. For instance, an abrupt difference in deflection (7 mm) can be seen between LVDT19 and LVDT24 at the bottom flanges in Fig. 11 for load position 2. The same deformation incompatibility can also be seen in the FE analyses, albeit at a lower level (see Fig.11). The difference between the FE results and the test results is attributed to the boundary conditions adopted in the FE model and the incomplete connection fit in the test specimen. In the FE model, the uplift of the specimen was locked and the connection modules were modelled with a perfect fit between one another. In the performed tests, the specimen was free to displace upwards and gaps were present between the connection modules.

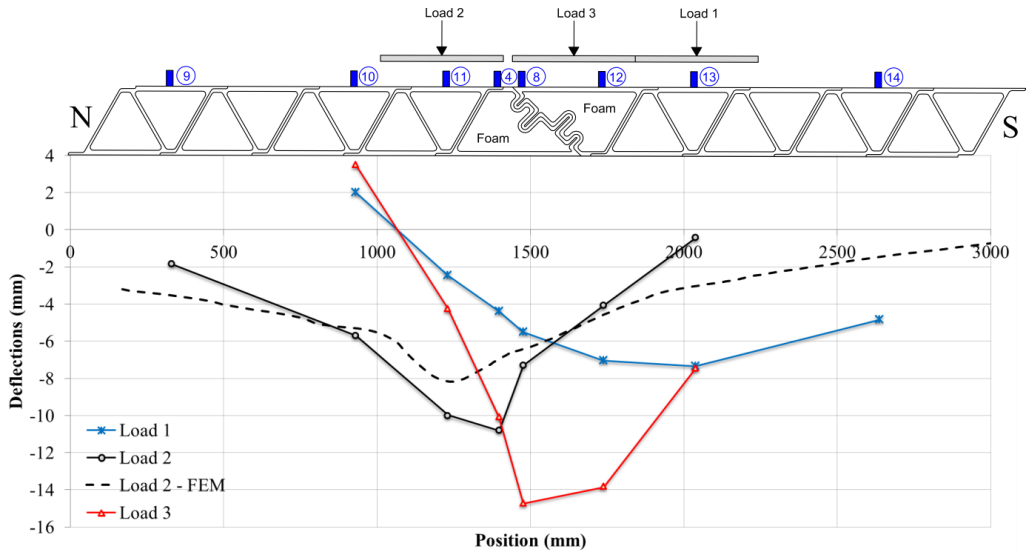

Fig. 10. Measured deflections at the top flanges in the transverse direction for SLS tests and comparison with FEM results for load position 2.

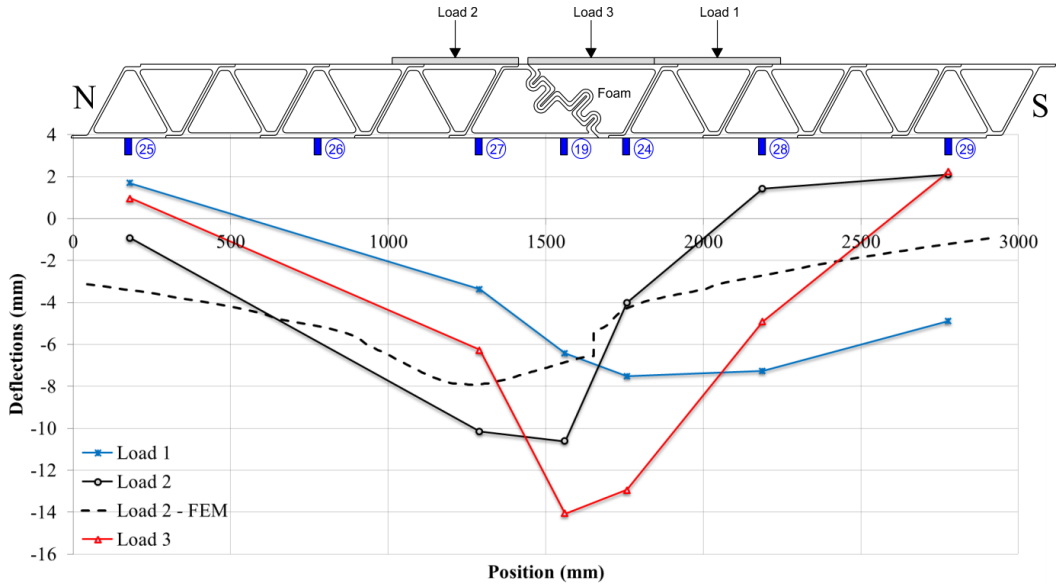

Fig. 11. Measured deflections at the bottom flanges in the transverse direction for SLS tests and comparison with FEM results for load position 2.

Due to the presence of gaps between the two connection modules (see Fig. 12), deformation incompatibility can also be seen at the top flanges (see LVDT4 and LVDT8 for load position 2 in Fig. 10), something that is not observed in the FE results. During loading, the connection modules rotated until the top flanges came into contact, as shown in Fig. 12.

Fig. 12. The presence of gaps between the connection modules and rotation of the specimen during loading.

This behaviour of the connection can be represented by a non-linear spring with intermediate stiffness, as illustrated in Fig. 13. The deflections of a loaded beam are shown in the figure for three principal cases. The spring behaviour of the connection accentuated the uplift of the specimen as well.

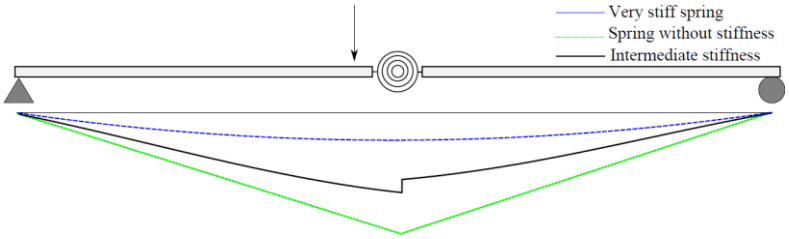

Fig. 13. Deflections of a beam with a spring with high, intermediate and no stiffness.

The relative movement of the top flanges might represent a threat for wear surface cracking. As reported in several studies [11, 17, 28-33], one problem of the constructed bridges with FRP decks is the cracking and delamination of the wear surface. In order to ensure the integrity of the wear surface, the relative movements of the connection modules should be prevented. In this study, the relative movements of the top flanges are attributed to the gaps of the connection. Thus, future research encompassing specimens of a higher level of precision and an applied wear surface with this type of connection is suggested. In addition, the load should be applied with a simulated tyre patch load in order to capture the local effects of the load, which are of more importance in the study of the wear surface cracking.

The transverse deflection patterns depicted in Fig. 11 also correspond well with the distribution of the support reactions during the tests. The west and east support reactions (see Fig. 7) show the same pattern and, in Fig. 14, the support reactions of the west support rollers are shown. The support reaction forces could be derived from the measured strains for an applied load up to 100 kN, because at higher loads yielding of the steel rollers occurred.

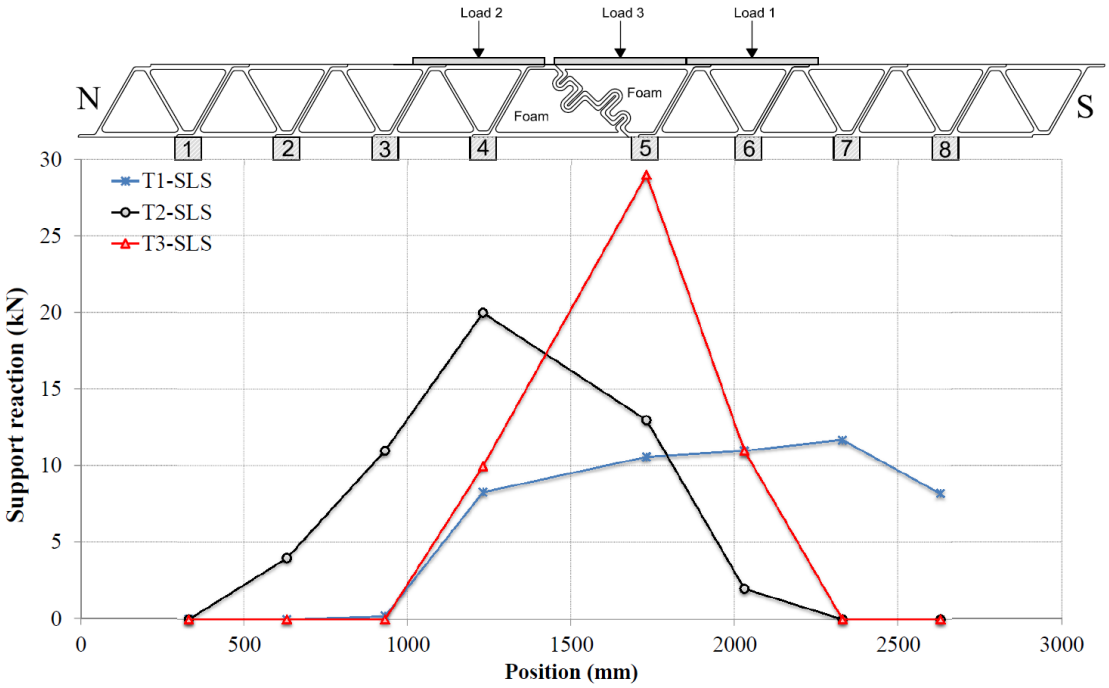

Fig. 14. Computed support reactions in the west support rollers for SLS tests at an applied load of 100 kN.

As noted in Fig. 14, the support reactions are mostly carried by the supports in the applied load area and the supports in the north or south part of the specimen do not carry any load, due to the fact that the specimen lifted in the north and south parts during loading according to the load position (see the transverse deflections in Fig. 11). This shows that the applied load is mainly distributed in the longitudinal direction (pultrusion direction of the ASSET deck) of the specimen, as illustrated in Fig. 15. In addition, the support reactions indicate the width of the specimen contributing to the load-carrying capacity for each load position. This width is referred to as effective width in this context. It is noted that the effective width of the specimen is the highest for the T1-SLS test and the lowest for the T3-SLS test.

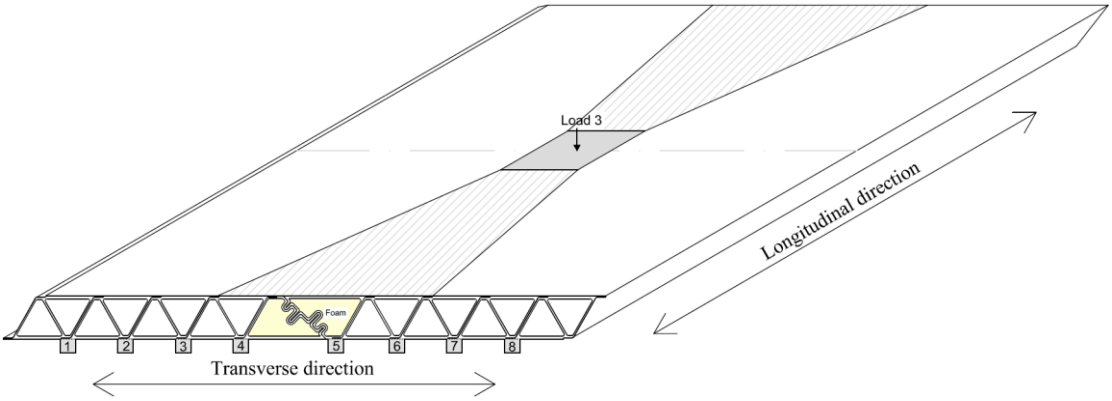

Fig. 15. Illustration of the load distribution area for load position 3.

The distribution of the support reactions in Fig. 14 indicates that the connection was able to transfer the loads through shear via the tongue-and-groove mechanism. For instance, in the T3-SLS test, the support reactions of supports No. 4 and No. 6 are almost the same, which shows that the load is transferred at the same rate to support 4 through the connection as it is to support 6. This performance contradicts the observations of the deflection incompatibilities in the transverse direction of the specimen shown in Fig. 10 and Fig. 11. However, this can be attributed to the opening of the connection modules, which is also discussed later. In the mid-span, the connection modules were able to separate and open more than along the support lines.

The load-deflection curves for the three load cases are shown in Fig. 16. For load case 1 (T1-SLS), the behaviour of the specimen is linear. The load-deflection curves of the T2-SLS and T3-SLS tests show a slightly non-linear pattern. This non-linearity can be attributed to the opening of the connection modules during loading. For instance, in the T2-SLS test, a while after the load was applied, the north part of the connection could not pull down the south part of the connection and separation between the connection modules occurred. This separation resulted in loss of stiffness (see Fig. 18) and affected the load-deflection curve for the T2-SLS test in a non-linear pattern.

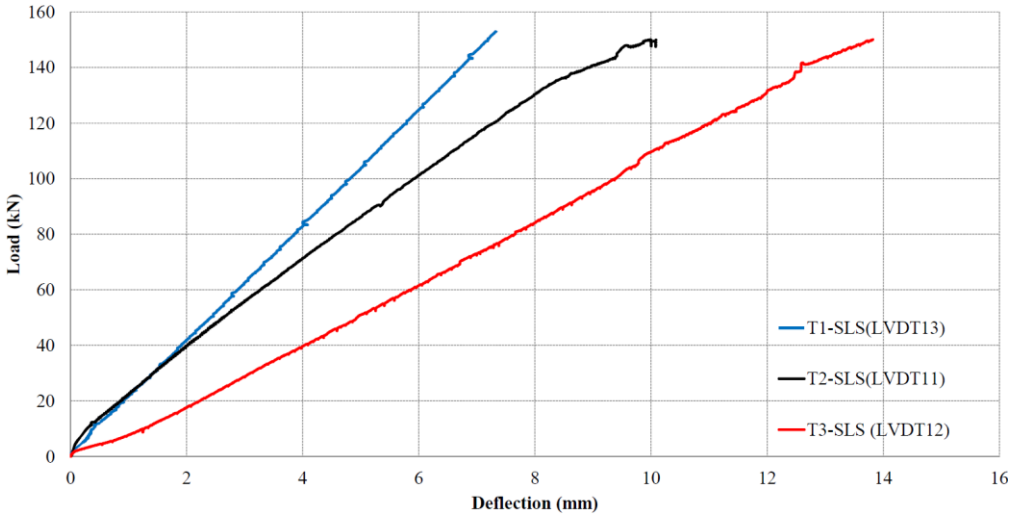

Fig. 16. Load-deflection curves for the SLS tests.

It is noted in Fig. 16 that the stiffness of the specimen is different for the three SLS tests. This difference in stiffness is attributed to several reasons:

- The load-deflection curves are given for different load positions and the deflections vary according to the load position. For instance, when comparing the deflections for the load positions 1 and 2 (refer to Fig. 10); the deflections for the load position 2 are higher because of the separation between the connection modules.
- The effective width of the specimen carrying the applied loads for each SLS tests can be directly related to the stiffness of the specimen. It is noted in Fig. 14 that the effective width of the specimen is the lowest for the T3-SLS test. This can be correlated to the stiffness of the specimen in the T3-SLS test which shows the lowest stiffness.
- The difference in the material properties and the geometric configuration between the ASSET deck and the connection modules can also be associated to the different stiffness values for each load position. For instance, the flange thickness of the connection module varied from 8 to 10 mm whereas the flange thickness of the ASSET deck was 15.6 mm. To this end, the local deflections of the connection modules would be higher than those of the ASSET deck.
- The residual openings of the connection modules (which are described in the following), in particular for T2-SLS (refer to Fig. 18), could also have influenced the stiffness of the subsequent test.

The relative horizontal displacements – which are referred to as openings in this context – were measured at the bottom flanges of the connection modules, in locations where the connection tends to open, along the span of the specimen (see Fig. 9 and Fig. 17).

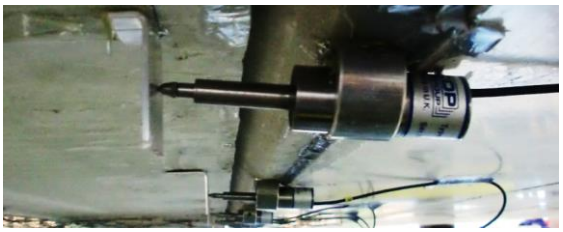

Fig. 17. Configuration of the LVDTs to measure the relative horizontal displacements (openings) between the connection modules at the bottom.

The load-opening curves in the mid-span of the specimen for each load case are shown in Fig. 18. For each load case, all the other LVDTs measuring the openings showed the same behaviour as the ones depicted in Fig. 18. However, the measured openings toward the support lines were approximately 35% lower.

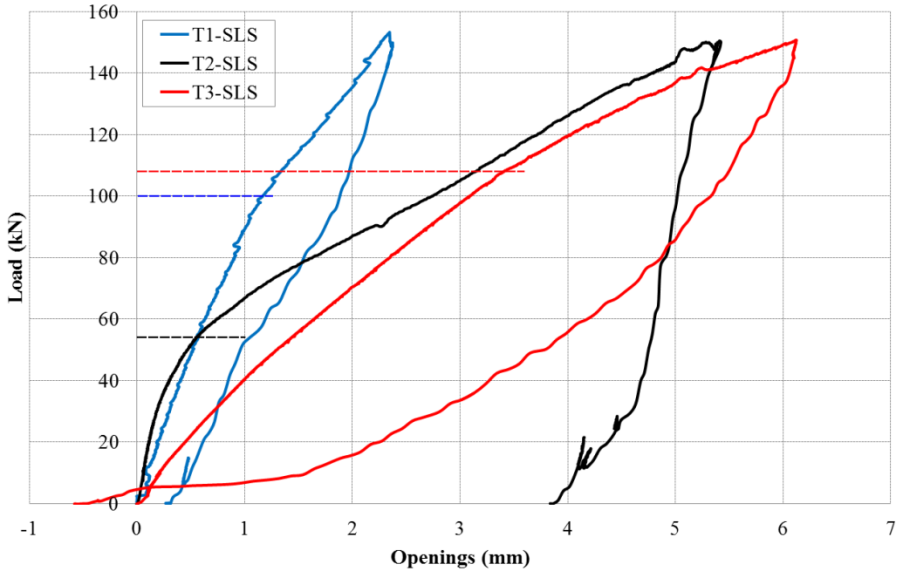

Fig. 18. Load-opening curves in the mid-span for the SLS tests.

All the tests in Fig. 18 display ‘two-phase’ stiffness behaviour (indicated by dotted lines in Fig. 18), which is more pronounced for the T2-SLS test. The stiffness of the connection in the T2-SLS test is slightly higher than in the T1-SLS test up to approximately 55 kN, after which it is considerably reduced. This decrease is due to the opening and separation of the connection modules and the loss of friction between the connection surfaces. After unloading, the highest residual openings were recorded for the T2-SLS test, which influenced the stiffness of the connection in the T3-SLS test as well. The residual openings of the connection in this study are mainly attributed to the flaws and the inappropriate fit between the tongues and grooves of the connection. As already mentioned previously, the connection modules rotated during loading due to the presence of the gaps. Owing to this rotation, while the bottom flanges were opening, the top flanges of the connection modules were closing. The closures and openings were measured manually during the tests. Hence, the rotation of the connection modules influenced the openings, which could not be entirely retrieved as the specimen was unloaded, in particular for the T2-SLS test. Part of the residual openings could also be attributed to the possible internal damages of the tongues and grooves. During loading, slight crack sounds were heard, but no visible damage was detected. After unloading in the T3-SLS test, it can be seen that the opening returned to approximately –0.5 mm, which indicates that part of the residual opening from load position 2 was actually recovered after T3-SLS. This

recovery was reflected in the higher stiffness of the specimen in the T3-Fail test, which is described in Section 4.5.2.

The measured strain in the longitudinal direction of the specimen at load 150 kN for T1-SLS is illustrated in Fig. 19. This figure is also representative of the other two tests, as the pattern of the strain distribution is the same.

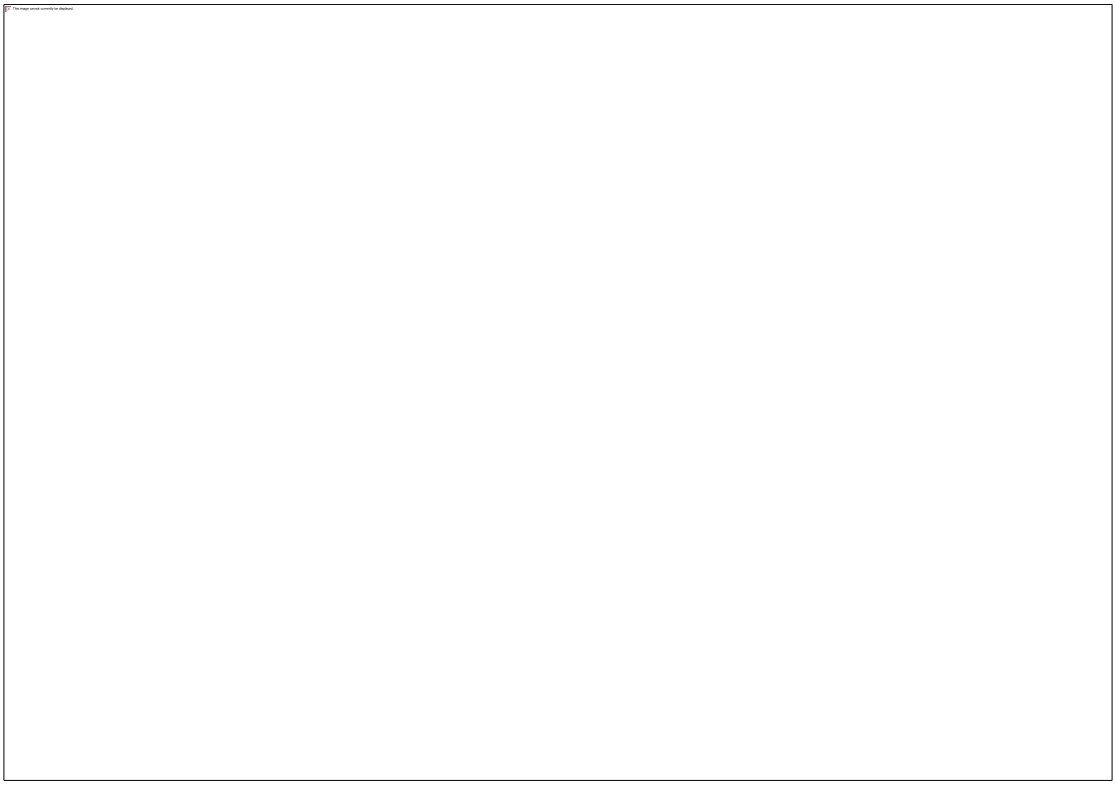

Fig. 19. Distribution of the measured axial strain in the longitudinal direction for T1-SLS.

One interesting observation from all the tests is that the longitudinal strain on the top flange in line with the applied load decreases close to the load location instead of increasing (marked in a circle in Fig. 19). This behaviour is attributed to the local bending effect of the flanges. When the specimen is loaded in bending, the top flanges and bottom flanges are subjected to compression and tension respectively, due to global bending action. The top thin flange is also subjected to extra local bending due to the patch load. This local bending would be even more pronounced with tyre loads as demonstrated in several studies [34, 35], which should be taken into account in studies of wear surface cracking. The secondary stresses due to this local action are depicted in Fig. 20. This behaviour was also verified in the numerical models developed to analyse the behaviour of the specimen.

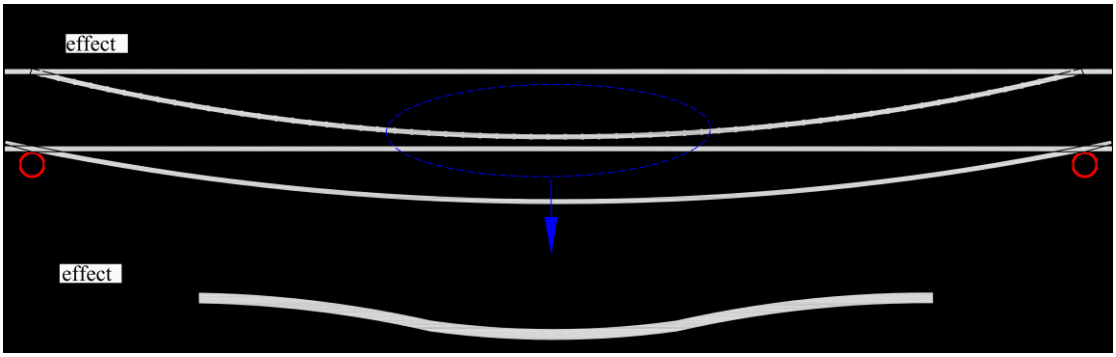

Fig. 20. Local loading effect on the strain.

Based on the measured strain, the maximum stress in the ASSET deck was calculated using the following matrix:

$$\begin{Bmatrix}\sigma_L\\ \sigma_T\end{Bmatrix}=\begin{bmatrix}\dfrac{E_L}{1-\nu_{LT}\nu_{TL}} & \dfrac{\nu_{TL}E_L}{1-\nu_{LT}\nu_{TL}}\\ \dfrac{\nu_{LT}E_T}{1-\nu_{LT}\nu_{TL}} & \dfrac{E_T}{1-\nu_{LT}\nu_{TL}}\end{bmatrix}\begin{Bmatrix}\varepsilon_L\\ \varepsilon_T\end{Bmatrix} \quad (1)$$

where *L* represents the longitudinal (pultrusion) direction and *T* the transverse direction.

The maximum stresses obtained for all load positions in the longitudinal and transverse directions are summarised in Table 5. It can be seen that the computed stress is much lower than the strength of the flanges of the ASSET deck. The stresses are lower than 20% of the tensile strength of the material, which is a value referred to as a limit for the performance of FRP materials under sustained plus fatigue service loads by Coogler et al. [36]. Due to the lack of material data, the stress computed for the connection modules could not be compared with the strength.

Table 5. Computed stress in the flanges of the ASSET deck and the connection modules and the strength properties (all units in MPa).

	ASSET deck								Connection module			
	Top flange		Bottom flange		Strength				Top flange		Bottom flange	
	σ_L	σ_T	σ_L	σ_T	f_{Lu} *	f_{Tu}	f_{cLu} *	f_{cLu}	σ_L	σ_T	σ_L	σ_T
T1-SLS	-6.3	-7.9	15.6	2.5	300	220	-250	-200	-14.7	-8.3	3.3	-0.3
T2-SLS	-7	-10.5	19.5	10.4					-4.6	1.0	20.0	9.1
T3-SLS	-13.6	-0.5	18.6	2.4					-11.4	-11.8	7.1	1.4

*L: longitudinal direction, T: transverse direction, f_{Lu}, f_{Tu}: tensile strengths, f_{cLu}, f_{cTu}: compression strengths

4.4.2 Results of T3-Fail

The objective of this test was to study the behaviour, load-carrying capacity and failure mode of the specimen at load position 3. However, due to the load-capacity limits of the hydraulic jack, the specimen was loaded up to a maximum load of 433 kN and the test was stopped.

The results of the vertical deflection in the transverse direction of the specimen are shown in Fig. 21. In the T3-Fail test, only the transducers on the top flange were utilised. LVDT 9 and 14 did not provide results during the entire test. The deflections are shown for three different loads: SLS load (150 kN), ULS load (202.5 kN) and at the final load of 430 kN. The results indicate that, as the load increases, the deflection localises under the load area. This local deflection is also observed from the finite element analyses, presented in Fig. 21 at the 430 kN load.

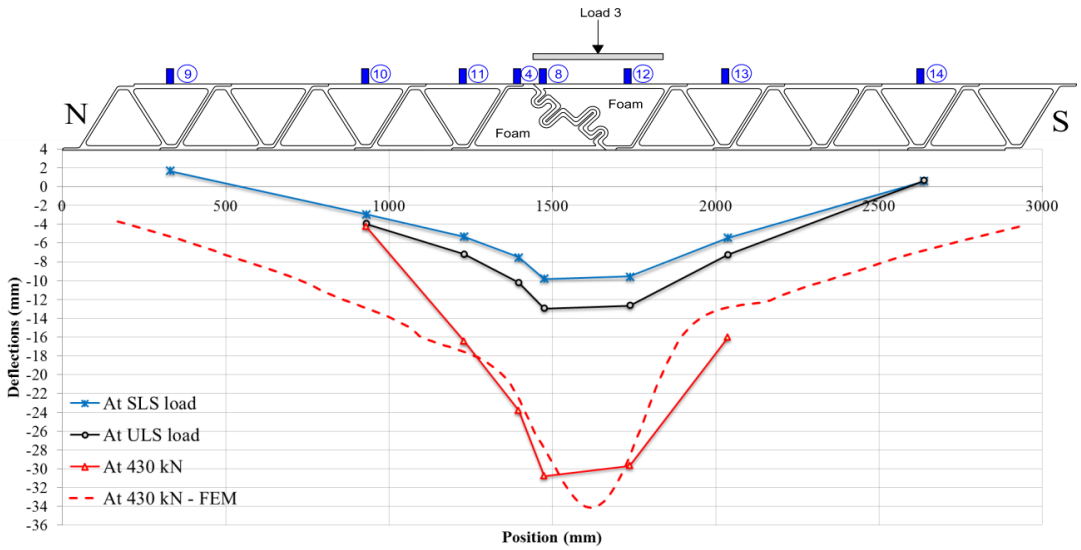

Fig. 21. Measured vertical deflection in the transverse direction for the final test and comparison with the FEM results at a load of 430 kN.

The measured load-deflection behaviour of the specimen up to a load of 433 kN on the upper flange (LVDT 12) is shown in Fig. 22. The load-deflection curve was compared with the one from the SLS test for the same load position (T3-SLS) and it was observed that the stiffness in the final test was higher. This higher stiffness can be attributed to the closure of the connection in T3-SLS after unloading, as presented in Section 4.4.1 (see Fig. 18). In the T3-SLS test, after unloading, the tongue and grooves of the connection fitted better than in the beginning of the test. The friction area between the connection modules was therefore increased, which reflected in approximately 35% higher stiffness in the T3-Fail test compared with the T3-SLS test. This indicates that the openings and closures between the connection modules are attributed to the gaps, movements and rotations between the connection modules depending on the load position and not to any damage of the modules during the SLS tests. The load-deflection curve for the T3-Fail test is also compared with the FE results in Fig. 22.

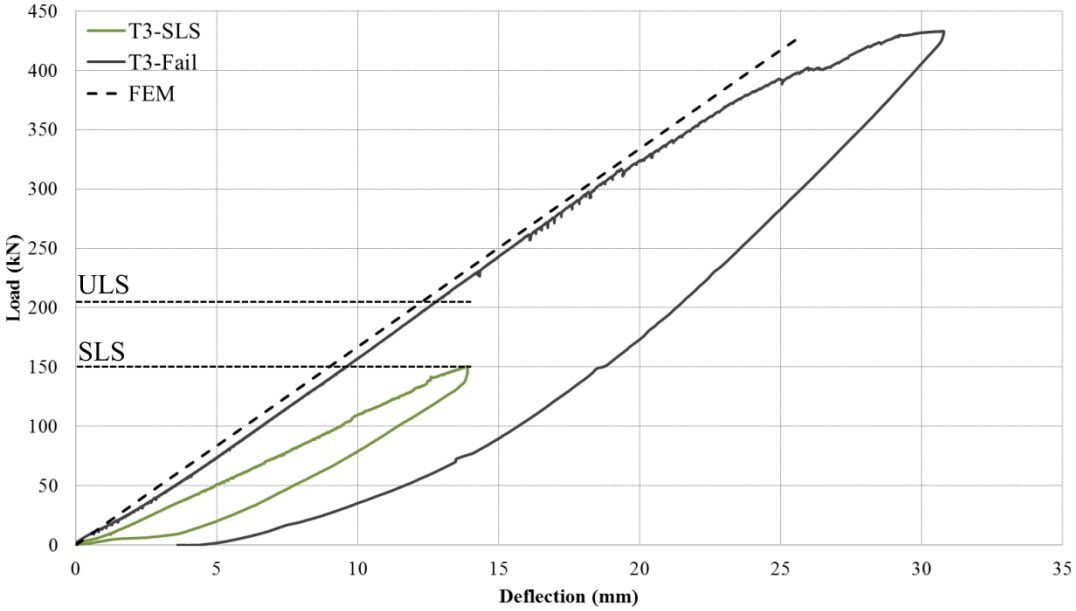

Fig. 22. Load-deflection curves for the top flange of the final test compared with the T3-SLS test and FEM results.

In the FE results, the load-deflection curve is linear, whereas it shows a pattern of a weak S-curve in the T3-Fail test. The incorrect fit of the connection modules to one another is the main reason for the non-linearity of the curve up to a load of 300 kN. Between a load of 250 and 350 kN, small falls in load were observed in the curve from the test and continuous cracking sounds were heard. At a load of 315 kN, delamination was observed at the ASSET deck lap joints, as shown in Fig. 23. The ASSET deck distributes the loads through the webs in tension and compression due to its triangular shape. The webs in tension produce through-thickness tensile stresses that cause delamination failure of the lap joints in the ASSET deck.

Fig. 23. Delamination of the lap joint of the ASSET deck at a load of 315 kN.

Afterwards, the same type of delamination failure in the lap joints at different locations developed and the delaminations propagated as the load increased (see Fig. 24). All the delamination failures occurred in the FRP material of the lap joints and not in the adhesive layer, indicating that the through-thickness tensile strength of the FRP material is lower than that of the adhesives. This type of delamination failure is common for cellular FRP decks as it has also been observed in other studies [23, 24, 37].

Fig. 24. Propagation of delamination as the load increases.

Due to delamination failures, the stiffness of the specimen was reduced after the load of 315 kN, whereas the FE analyses reveal linear behaviour in Fig. 22. The FE analyses in this study were carried out using shell elements with a linear-elastic approach, which ignores the interlaminar shear stresses, through-thickness effects and progressive damage to the FRP material.

No failure was observed in the connection module up to a load of 426 kN. At this load level, separation of the ‘tongue’ from the bottom flange was observed at the supports (see Fig. 25). This separation propagated inwards up to a length of 350 mm. This failure mode indicates that it is the tensile strength of the flange that controls the strength of the connection module.

Fig. 25. Separation of the bottom flange from the 'tongue' of the connection module.

After a load of 400 kN, pseudo-ductile behaviour in the specimen can be seen in Fig. 22, but a maximum load of 433 kN could be reached when the specimen was unloaded. After unloading, the vertical deflection did not recover fully, but residual deflection of approximately 3 mm was observed.

Based on the measured strain, the maximum longitudinal and transverse stresses in the ASSET deck flanges and the connection module were computed at a load level of 430 kN and are summarised in Table 6. The maximum axial stresses for the ASSET deck are computed as -36.3 MPa in the top flange and 53.8 MPa in the bottom flange. These stresses are much lower than the strength of the flanges of the ASSET deck, but, as the failure mode indicates, it is the through-thickness tensile stresses which govern the failure of the ASSET deck.

Table 6. Computed stresses in the flanges of the ASSET deck and the strength properties at load level of 430 kN for the final test (all units in MPa).

T3-Fail	ASSET deck								Connection module			
	Top flange		Bottom flange		Strength				Top flange		Bottom flange	
	σ_L	σ_T	σ_L	σ_T	f_{Lu} *	f_{Tu}	f_{cLu} *	f_{cLu}	σ_L	σ_T	σ_L	σ_T
430 kN	-36.3	-4.8	53.8	15.3	300	220	-250	-200	-1.8	-4.7	33.6	12.0

*L: longitudinal direction, T: transverse direction, f_{Lu},f_{Tu}: tensile strengths, f_{cLu},f_{cTu}: compression strengths

5. Discussion

It was of interest to compare the behaviour of the deck encompassing the developed connection with the behaviour of a deck without the connection. Hence, finite element analyses were carried out and a comparison of the global deflections for the two cases was made at the SLS load, as depicted in Fig. 26.

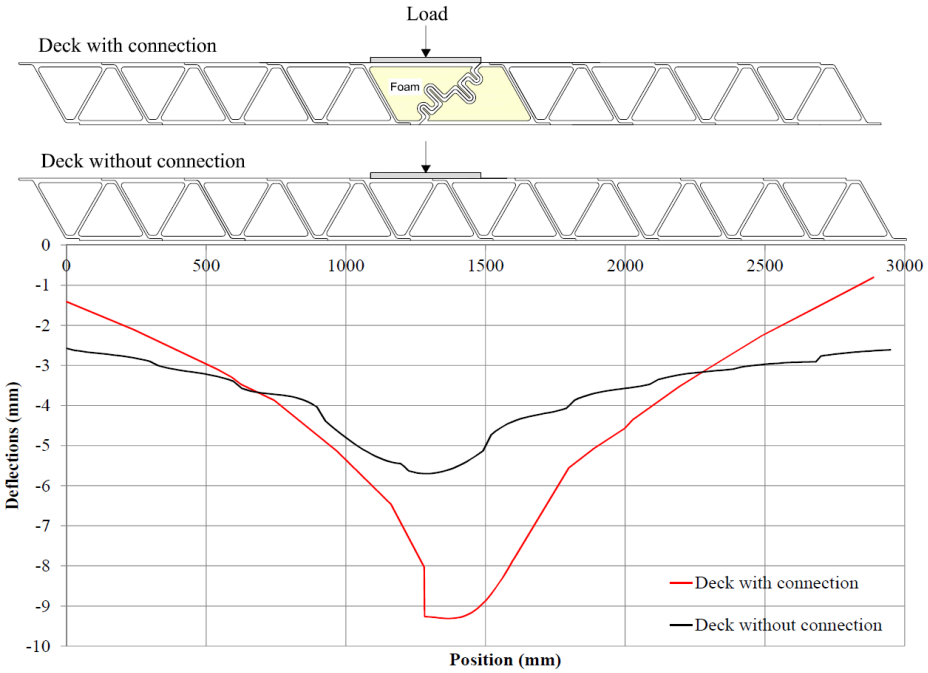

Fig. 26. Comparison of the global deflection of the deck with and without the connection.

It is noted that the behaviour of the deck with and without a connection is to some extent different. The deflections of the deck without connection are uniform with a certain localised deflection in the load application area. The pattern of the deflection curve for the deck with the connection has a V-shape with more localised deflections in the load application area. The global deflections tend to significantly decrease toward the edges of the specimen for the deck with the connection. This is attributed to the spring behaviour of the connection. As already discussed in Section 4.4.1, the behaviour of the connection is analogous to a spring with intermediate stiffness, which is between a spring with high stiffness and a spring with no stiffness (hinge). To decrease this behaviour of the connection, modification of the tongue and grooves can be considered. Nevertheless, the deflections of the deck with the connection are lower that the limit of L/300 and this type of connection offers advantages over bonding, such as swift on-site assembly and ease of disassembly, which should not be overlooked.

6. Summary and conclusions

In this study, a novel connection was proposed for the potential rapid on-site assembly of fibre reinforced polymer bridge deck panels. The connection development process from conceptual design to verification through testing is described in this paper.

The finite element method was used to perform a detailed design of the connection and to investigate the structural behaviour. The FE analyses showed promising results for the connection concept. The deflection limits were met in the serviceability limit state and the stresses were fairly low compared with the ultimate strength of the material.

Subsequently, the connection modules were manufactured using a vacuum infusion process. Due to the geometric complexity of the connection concept, the vacuum infusion process failed to produce connection modules which fit completely between one another. In the future, it is suggested that the connection configuration should be

produced by pultrusion as a manufacturing method instead of vacuum infusion. Production with pultrusion would provide regular, accurate geometries with minimum tolerances. In spite of the flaw between the connection modules, the results of the static experimental tests, which were performed to verify the design and study the behaviour and the load-carrying capacity of the connection, were acceptable with regard to strength and stiffness.

Three static tests up to a load of 150 kN (SLS load) in different load positions were carried out on a specimen consisting of two FRP deck (ASSET deck) panels which were joined by the developed connection modules. The load-deflection responses were mainly linear elastic with slight non-linearity and this was attributed to the openings and flaws between the connection modules. The maximum deflection ratio was recorded as span/214.

A final test was carried out on the specimen up to a load of 433 kN. The load-deflection curve of the specimen showed the pattern of a weak S-curve. At a load of 312 kN, progressive delamination between the fibre lay-ups started at the flange-web intersections of the FRP deck due to through-thickness tensile stresses. After the delamination failures in the deck, the behaviour of the specimen was slightly non-linear and, after a load of 400 kN, pseudo-ductile behaviour was observed. The test was terminated at 433 kN without failure occurring in the specimen. As a result, the failure load of the specimen is higher than 433 kN, which is larger than the ULS load (202.5 kN).

In overall terms, the results of this study show that the proposed connection has good potential for use in FRP decks. However, additional experimental studies encompassing specimens with a higher level of precision are recommended to obtain enhanced performance in the serviceability limit state. In addition, the fatigue performance and the environmental effects on the durability of the connection should be investigated.

Acknowledgements

The work presented in this paper is part of the EU-funded PANTURA project [38]. The authors would like to acknowledge the assistance and support provided by Fiberline Composites (Denmark) and Mostostal Warszawa S.A. (Poland), the manufacturers of the test specimens. Thanks are also given to ACCIONA Infraestructuras S.A. (Spain) for their involvement in the conceptual design phase.

References

1. Luke S, Canning L, Collins S, Knudsen E, *et al.* Advanced composite bridge decking system - Project ASSET. Structural Engineering International: Journal of the International Association for Bridge and Structural Engineering (IABSE), 2002; 12(2): p. 76-79.
2. Canning L, Luke S. Development of FRP bridges in the UK - An overview. Advances in Structural Engineering, 2010; 13(5): p. 823-835.
3. Knippers J, Pelke E, Gabler M, Berger D. Bridges with glass fibre-reinforced polymer decks: The road bridge in Friedberg, Germany. Structural Engineering International: Journal of the International Association for Bridge and Structural Engineering (IABSE), 2010; 20(4): p. 400-404.

4. Van Erp G, Cattell C, Ayers S. A fair dinkum approach to fibre composites in civil engineering. Construction and Building Materials, 2006; 20(1-2): p. 2-10.
5. Lewis A E, Dumlao C, Lee M J, Weinmann T L. Performance of Schuyler Heim composite Bridge deck replacement port of Los Angeles, California. 2004, Transportation Research Record. p. 36-46.
6. Lee S W, Hong K J, Park S. Current and future applications of glass-fibre-reinforced polymer decks in Korea. Structural Engineering International: Journal of the International Association for Bridge and Structural Engineering (IABSE), 2010; 20(4): p. 405-408.
7. Sams M. Broadway bridge case study bridge deck application of fiber-reinforced polymer. In: Transportation Research Board - 6th International Bridge Engineering Conference: Reliability, Security, and Sustainability in Bridge Engineering, Boston, United States, 2005.
8. Hota G V S, Hota S R V. Advances in fibre-reinforced polymer composite bridge decks. Progress in Structural Engineering and Materials, 2002; 4: p. 161-168.
9. Solomon G, Godwin G. Expanded use of composite deck projects in USA. Structural Engineering International: Journal of the International Association for Bridge and Structural Engineering (IABSE), 2002; 12(2): p. 102-104.
10. Cassity P, Richards D, Gillespie J. Compositely acting FRP deck and girder system. Structural Engineering International: Journal of the International Association for Bridge and Structural Engineering (IABSE), 2002; 12(2): p. 71-75.
11. Fu C C, Alayed H, Amde A M, Robert J. Field performance of the fiber-reinforced polymer deck of a truss bridge. Journal of Performance of Constructed Facilities, 2007; 21(1): p. 53-60.
12. Turner M K, Harries K A, Petrou M F, Rizos D. In situ structural evaluation of a GFRP bridge deck system. Composite Structures, 2004; 65(2): p. 157-165.
13. Alampalli S, O'Connor J, Yannotti A P. Fiber reinforced polymer composites for the superstructure of a short-span rural bridge. Composite Structures, 2002; 58(1): p. 21-27.
14. Alampalli S, Kunin J. Rehabilitation and field testing of an FRP bridge deck on a truss bridge. Composite Structures, 2002; 57(1-4): p. 373-375.
15. Mara V, Haghani R, Harryson P. Bridge decks of fibre reinforced polymer (FRP): A sustainable solution. Construction and Building Materials, 2014; 50(0): p. 190-199.
16. Zhou A, Keller T. Joining techniques for fiber reinforced polymer composite bridge deck systems. Composite Structures, 2005; 69(3): p. 336-345.
17. Alampalli S. Field performance of an FRP slab bridge. Composite Structures, 2006; 72(4): p. 494-502.
18. Liu Z, Majumdar P K, Cousins T E, Lesko J J. Development and evaluation of an adhesively bonded panel-to-panel joint for a FRP bridge deck system. Journal of Composites for Construction, 2008; 12(2): p. 224-233.
19. Zi G, Kim B M, Hwang Y K, Lee Y H. An experimental study on static behavior of a GFRP bridge deck filled with a polyurethane foam. Composite Structures, 2008; 82(2): p. 257-268.
20. http://www.fiberline.com/structures/profiles-and-decks-bridges/profiles-road-bridges/bridge-decks-heavy-loads/fbd600-asset-br/fbd600-asset-bridge-deck-pr.

21. Clarke J L. Structural Design of Polymer Composites: Eurocomp Design Code and Background Document. Taylor & Francis, 2003.
22. (CEN). Eurocode 1: Actions on structures - Part 2: Traffic loads on bridges. 2003; EN 1991-2:2003.
23. Keller T, Schollmayer M. Plate bending behavior of a pultruded GFRP bridge deck system. Composite Structures, 2004; 64(3-4): p. 285-295.
24. Canning L, Hodgson J, Karuna R, Luke S, *et al.* Progress of advanced composites for civil infrastructure. Proceedings of the Institution of Civil Engineers: Structures and Buildings, 2007; 160(6): p. 307-315.
25. Sebastian W M, Webster T, Kennedy C, Ross J. Profiled metal plate - Cork mat loading systems on cellular FRP bridge decks to reproduce tyre-to-deck contact pressure distributions. Construction and Building Materials, 2013.
26. Majumdar P K, Lesko J J, Cousins T E, Liu Z. Conformable tire patch loading for FRP composite bridge deck. Journal of Composites for Construction, 2009; 13(6): p. 575-581.
27. Brown D L, Berman J W. Fatigue and strength evaluation of two glass fiber-reinforced polymer bridge decks. Journal of Bridge Engineering, 2010; 15(3): p. 290-301.
28. Berman J W, Brown D L. Field monitoring and repair of a glass fiber-reinforced polymer bridge deck. Journal of Performance of Constructed Facilities, 2010; 24(3): p. 215-222.
29. Reising R M W, Shahrooz B M, Hunt V J, Neumann A R, *et al.* Performance comparison of four fiber-reinforced polymer deck panels. Journal of Composites for Construction, 2004; 8(3): p. 265-274.
30. Hong T, Hastak M. Construction, inspection, and maintenance of FRP deck panels. Journal of Composites for Construction, 2006; 10(6): p. 561-572.
31. Canning L. Performance and 8-year load test on West Mill FRP Bridge. In: CICE 2012, Rome, Italy, 2012.
32. Canning L, Luke S, Brown P. Structural monitoring and 8-year load test on Europe's first fibre-reinforced polymer highway bridge. Proceedings of the ICE - Bridge Engineering, 2013: p. 1-6.
33. Triandafilou L N, O'Connor J S. Field issues associated with the use of fiber-reinforced polymer composite bridge decks and superstructures in harsh environments. Structural Engineering International: Journal of the International Association for Bridge and Structural Engineering (IABSE), 2010; 20(4): p. 409-413.
34. Sebastian W M, Keller T, Ross J. Influences of polymer concrete surfacing and localised load distribution on behaviour up to failure of an orthotropic FRP bridge deck. Composites Part B: Engineering, 2013; 45(1): p. 1234-1250.
35. Majumdar P K, Liu Z, Lesko J J, Cousins T E. Performance evaluation of FRP composite deck considering for local deformation effects. Journal of Composites for Construction, 2009; 13(4): p. 332-338.
36. Coogler K, Harries K A, Wan B, Rizos D C, *et al.* Critical evaluation of strain measurements in glass fiber-reinforced polymer bridge decks. Journal of Bridge Engineering, 2005; 10(6): p. 704-712.
37. Keller T, Gürtler H. In-plane compression and shear performance of FRP bridge decks acting as top chord of bridge girders. Composite Structures, 2006; 72(2): p. 151-162.
38. http://www.pantura-project.eu/.